

## LONG RANGE HADRON DENSITY FLUCTUATIONS AT SOFT $P_T$ IN AU+AU COLLISIONS AT RHIC

MIKHAIL L. KOPYTINE

*Department of Physics, Kent State University, USA*

FOR THE STAR COLLABORATION

Dynamic fluctuations in the local density of non-identified hadron tracks reconstructed in the STAR TPC are studied using the discrete wavelet transform power spectrum technique which involves mixed event reference sample comparison. The two-dimensional event-by-event analysis is performed in pseudo-rapidity  $\eta$  and azimuthal angle  $\phi$  in bins of transverse momentum  $p_T$ . HIJING simulations indicate that jets and mini-jets result in characteristic signals, visible already at soft  $p_T$ , when the dynamic texture analysis is applied. In this analysis, the discrepancy between the experiment and the HIJING expectations for Au+Au at  $\sqrt{S_{NN}} = 200$  GeV is most prominent in the central collisions where we observe the long range fluctuations to be enhanced at low  $p_T$ , and suppressed above  $p_T = 0.6$  GeV

### 1. Introduction

The on-going RHIC program, motivated by an interest in the bulk properties of strongly interacting matter under extreme conditions, has already yielded a number of tantalizing results. Deconfinement and chiral symmetry restoration<sup>1</sup> are expected to take place in collisions of ultra-relativistic nuclei. Because these phase transitions are multiparticle phenomena, a promising, albeit challenging, approach is the study of dynamics of large groups of final state particles. The dynamics shows itself in the correlations and fluctuations (texture) on a variety of distance scales in momentum space.

The multi-resolution dynamic texture approach (applied for the first time<sup>2</sup> at SPS) uses discrete wavelet transform<sup>3</sup>(DWT) to extract such information. At the present stage, the information is extracted in a comprehensive way, without any built-in assumptions or filters. Mixed events are used as a reference for comparison in search for dynamic effects. Event generators are used to “train intuition” in recognizing manifestations of familiar physics (such as elliptic flow or jets) in the analysis output, as

well as to quantify sensitivity to the effects yet unidentified, such as critical fluctuations or clustering of new phase at hadronization.

## 2. The STAR experiment

The STAR Time Projection Chamber<sup>4</sup>(TPC) is mounted inside a solenoidal magnet. It tracks charged particles within a large acceptance ( $|\eta| < 1.3$ ,  $0 < \phi < 2\pi$ ) and is well suited for event-by-event physics and in-depth studies of event structure. The data being reported are obtained during the second ( $\sqrt{S_{NN}} = 200$  GeV) year of RHIC operation. The minimum bias trigger discriminates on a neutral spectator signal in the Zero Degree Calorimeters<sup>5</sup>. By adding a requirement of high charged multiplicity within  $|\eta| < 1$  from the scintillating Central Trigger Barrel, one obtains the central trigger. Vertex reconstruction is based on the TPC tracking. Only high quality tracks found to pass within 3 cm of the event vertex are accepted for the texture analysis.

## 3. Dynamic texture analysis procedure

Discrete wavelets are a set of functions, each having a proper width, or scale, and a proper location so that the function differs from 0 only within that width and around that location. The set of possible scales and locations is discrete. The DWT transforms the collision event in pseudo-rapidity  $\eta$  and azimuthal angle  $\phi$  into a set of two-dimensional functions. The basis functions are defined in the  $(\eta, \phi)$  space and are orthogonal with respect to scale and location. We accumulate texture information by averaging the power spectra of many events.

The simplest DWT basis is the Haar wavelet, built upon the *scaling function*  $g(x) = 1$  for  $0 \leq x < 1$  and 0 otherwise. The function

$$f(x) = \left\{ +1 \text{ for } 0 \leq x < \frac{1}{2}; -1 \text{ for } \frac{1}{2} \leq x < 1; 0 \text{ otherwise} \right\} \quad (1)$$

is the wavelet function.

The experimental acceptance in  $\eta, \phi$ , and  $p_T$  ( $(|\eta| < 1, 0 < \phi < 2\pi)$ ) is partitioned into bins. The  $\eta$ - $\phi$  partitions are of equal size, whereas in  $p_T$ , the binning is exponential when more than one  $p_T$  bin is used. In each bin, the number of reconstructed tracks satisfying the quality cuts is counted.

The scaling function of the Haar basis in two dimensions (2D)  $G(\phi, \eta) = g(\phi)g(\eta)$  is just a bin's acceptance (modulo units). The wavelet functions

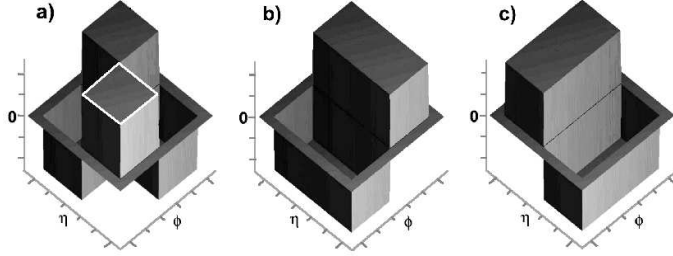


Figure 1. Haar wavelet basis in two dimensions. The three modes of directional sensitivity are: a) diagonal b) azimuthal c) pseudo-rapidity. For the finest scale used, the white rectangle drawn “on top” of the function in panel a) would correspond to the smallest acceptance bin (pixel). Every subsequent coarser scale is obtained by expanding the functions of the previous scale by a factor of 2 in both dimensions. (Reproduced from <sup>2</sup>).

$F^\lambda$  (where the mode of directional sensitivity  $\lambda$  can be azimuthal  $\phi$ , pseudo-rapidity  $\eta$ , or diagonal  $\phi\eta$ ) are

$$F^{\phi\eta} = f(\phi)f(\eta), \quad F^\phi = f(\phi)g(\eta), \quad F^\eta = g(\phi)f(\eta). \quad (2)$$

We set up a two dimensional (2D) wavelet basis:

$$F_{m,i,j}^\lambda(\phi, \eta) = 2^m F^\lambda(2^m \phi - i, 2^m \eta - j), \quad (3)$$

where  $m$  is the integer scale fineness index,  $i$  and  $j$  index the positions of bin centers in  $\phi$  and  $\eta$ . Then,  $F_{m,i,j}^\lambda$  with integer  $m$ ,  $i$ , and  $j$  are known <sup>3</sup> to form a complete orthonormal basis in the space of all *measurable functions* defined on the continuum of real numbers  $L^2(\mathbb{R})$ . We construct  $G_{m,i,j}(\phi, \eta)$  analogously to Eq.3.

Fig. 1 shows the wavelet basis functions  $F$  in two dimensions. At first glance it might seem surprising that, unlike the 1D case, both  $f$  and  $g$  enter the wavelet basis in 2D. Fig. 1 clarifies this: in order to fully encode an arbitrary shape of a measurable 2D function, one considers it as an addition of a change along  $\phi$  ( $f(\phi)g(\eta)$ , panel (b)), a change along  $\eta$  ( $g(\phi)f(\eta)$ , panel (c)), and a saddle-point pattern ( $f(\phi)f(\eta)$ , panel (a)), added with appropriate weight (positive, negative or zero), for a variety of scales. The finest scale available is limited by the two track resolution, and, due to the needs of event mixing, by the number of available events. The coarser scales correspond to successively re-binning the track distribution. The analysis is best visualized by considering the scaling function  $G_{m,i,j}(\phi, \eta)$  as binning the track distribution  $\rho(\phi, \eta)$  in bins  $i, j$  of fineness  $m$ , while the set of wavelet functions  $F_{m,i,j}^\lambda(\phi, \eta)$  (or, to be exact, the wavelet expansion

coefficients  $\langle \rho, F_{m,i,j}^\lambda \rangle$  gives the difference distribution between the data binned with given coarseness and that with binning one step finer. We use WAILI<sup>6</sup> software to obtain the wavelet expansions.

In two dimensions, it is informative to present the three modes of a power spectrum with different directions of sensitivity  $P^{\phi\eta}(m)$ ,  $P^\phi(m)$ ,  $P^\eta(m)$  separately. We define the **power spectrum** as

$$P^\lambda(m) = \frac{1}{2^{2m}} \sum_{i,j} \langle \rho, F_{m,i,j}^\lambda \rangle^2, \quad (4)$$

where the denominator gives the meaning of spectral density to the observable. So defined, the  $P^\lambda(m)$  of a random white noise field is independent of  $m$ . However, for physical events one finds  $P^\lambda(m)$  to be dependent on  $m$  due to the presence of **static texture** features such as acceptance asymmetries and imperfections (albeit minor in STAR), and non-uniformity of the  $dN/d\eta$  shape. In order to extract the **dynamic** signal, we use  $P^\lambda(m)_{true} - P^\lambda(m)_{mix}$  where the latter denotes power spectrum obtained from the **mixed events**. The mixed events are composed of the  $(\eta, \phi)$  pixels of true events, so that a pixel is an acceptance element of the finest scale used in the analysis, and in no mixed event is there more than one pixel from any given true event. The minimum granularity used in the analysis is  $16 \times 16$  pixels.<sup>a</sup>

Systematic errors can be induced on  $P^\lambda(m)_{true} - P^\lambda(m)_{mix}$  by the process of event mixing. For example, in events with different vertex position along the beam axis, same values of  $\eta$  may correspond to different parts of the TPC with different tracking efficiency. That will fake a dynamic texture effect in  $\eta$ . In order to minimize such errors, events are classified into **event classes** with similar multiplicity and vertex position. Event mixing is done and  $P^\lambda(m)_{true} - P^\lambda(m)_{mix}$  is constructed within such classes. Only events with  $z$  vertex lying on the beam axis within 25 cm from the center of the chamber are accepted for analysis. To form event classes, this interval is further subdivided into five bins. We also avoid mixing of events with largely different multiplicity. Therefore, another dimension of the event class definition is that of the multiplicity of high quality tracks in the TPC. For central trigger events, the multiplicity range of an event class is typically 50.

<sup>a</sup>For a quick reference, here are the scales in  $\eta$ . Scale 1:  $\Delta\eta = 1$ ; scale 2:  $\Delta\eta = 1/2$ ; scale 3:  $\Delta\eta = 1/4$  and so on.

#### 4. “Coherent” interference of patterns and normalization of power spectra

Imagine a reconstructed event as a distribution of points in the space of variables  $(\eta, \phi, p_T)$ . We slice this space into  $p_T$  bins and analyze two-dimensional  $(\eta, \phi)$  patterns. The patterns from different  $p_T$  slices of the same event will amplify the texture signal when those  $p_T$  bins are merged. Depending on how the amplification works, one will find different scaling law to relate the  $P^\lambda(m)_{true} - P^\lambda(m)_{mix}$  signal amplitude with the underlying number of particles.

The DWT power spectrum at each scale is (using Haar wavelet) a sum of squared pixel-to-pixel content differences for the given pixel fineness (scale). One can think of the pixel-to-pixel content difference the same way as one thinks of a random fluctuation in the pixel content. Imagine that the pattern being analyzed is a small sub-sample of the event, and its number of particles  $N$  can be increased at will, up to the point of making it an entire event – as is the case when the sub-sample is a  $p_T$  bin of the event. The pixel content will scale with  $N$ , and if the dynamic pattern preserves its shape from one  $p_T$  bin to another, the pixel-to-pixel difference on the characteristic scale of the pattern will also scale as  $N$ . Consequently, the dynamic component of the power spectrum for this scale will grow as  $N^2$ . We will call this behavior “coherent” in analogy with optics, where one needs coherence in order to see interference patterns.

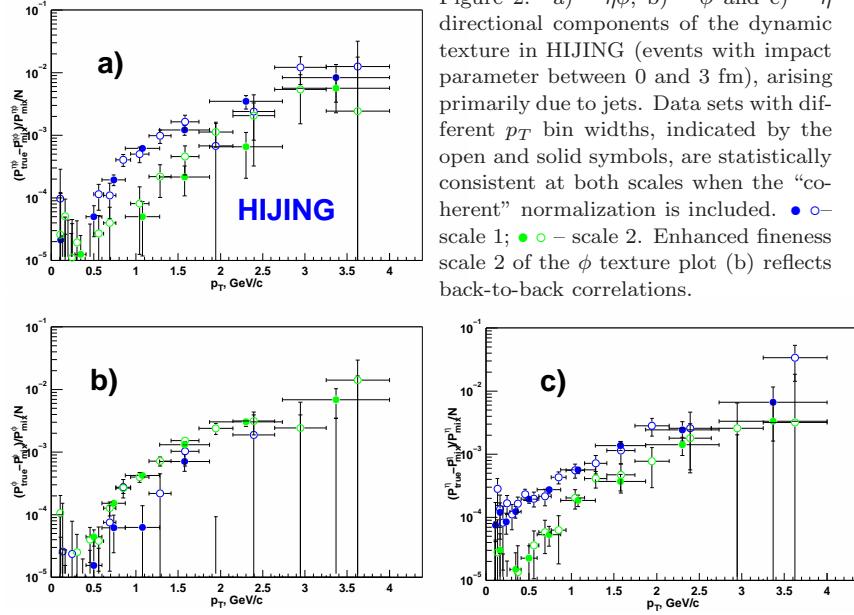
Normalization is needed in order to, first, express different measurements in the same units; second, eliminate trends in  $p_T$  dependence which are induced by the design of the measure and unrelated to the physics. For the “coherent” case, the normalized dynamic texture observable is

$$(P^\lambda(m)_{true} - P^\lambda(m)_{mix})/P^\lambda(m)_{mix}/N. \quad (5)$$

One could also imagine “incoherent”  $p_T$  slices. In the “incoherent” case, the pixel content will grow proportionally to  $N$ , but the pixel-to-pixel difference will grow as the RMS fluctuation of the pixel content, i.e. as the Poissonian  $\sqrt{N}$ . The dynamic component of the power spectrum will grow as  $N$  (i.e.  $\propto P(m)$ ) and

$$(P^\lambda(m)_{true} - P^\lambda(m)_{mix})/P^\lambda(m)_{mix} \quad (6)$$

should be used in this case. In the DWT-based texture analysis, amplification of the signal is based not on adding the patterns themselves, but on adding the power spectra of local density fluctuations, that is (continuing the optics analogy) adding the intensities rather than field amplitudes. For



this reason, in the DWT analysis one does not require “coherence” to amplify the signals from many  $p_T$  slices, just as in optics one does not need coherence to see the light intensity increase with an increase in the number of photons.

## 5. Textures of jets and critical fluctuations in event generators

Dynamic texture is to be expected from HIJING<sup>7</sup> given its particle production mechanism at RHIC energy (jets, mini-jets and string fragmentation). HIJING combines a perturbative QCD description at high  $p_T$  with a model of low  $p_T$  processes. Figure 2 demonstrates observability of the HIJING dynamic effects in our analysis.<sup>b</sup> We see that, first, the difference between the true and mixed events is noticeable and can be studied as a function of  $p_T$  with the present HIJING statistics of around  $1.6 \times 10^5$  events. Second,

<sup>b</sup>In all MC generators, no GEANT and no response simulation is done. Instead, only stable charged particles ( $e, \mu, \pi, K, p$ ) and their antiparticles from the generator output are considered, provided that they fit into the STAR TPC fiducial  $\eta$  acceptance  $|\eta| \leq 1$ . Momentum resolution and  $p_T$  acceptance are not simulated.

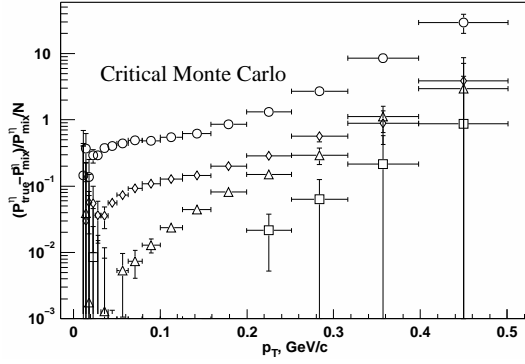


Figure 3.  $(P_{true}^{\eta} - P_{mix}^{\eta})/P_{mix}^{\eta}N$  from the Critical MC generator. Events with 20 to 30 charged tracks in the STAR acceptance are analyzed.  $\circ$  – scale 1,  $\diamond$  – scale 2,  $\triangle$  – scale 3,  $\square$  – scale 4.

the open and closed symbols, which correspond to different  $p_T$  bin sizes, appear to fall on the same curve after the  $1/N$  normalization, where  $N$  is a  $p_T$  bin multiplicity, as would be the case for “coherent” (see Section 4)  $p_T$  bins. Third, the rise of the signal with  $p_T$  is due to the fact that high  $p_T$  is dominated by jet production. As far as the  $p_T$  “coherence” is concerned, one would expect that a high  $p_T$  parton, creating hadrons via fragmentation, produces similar  $(\eta, \phi)$  patterns at different  $p_T$  as the energy sharing among the secondaries proceeds, and thus the coherent interference of  $p_T$  patterns is natural for this mechanism of particle production. These signals in HIJING are gone when jet production is turned off in the generator. Ability to study jet textures at soft, as well as high,  $p_T$  means that the study promises to be very informative because majority of the reconstructed tracks will be utilized.

CMC is Critical Monte Carlo generator created by N. Antoniou and coworkers<sup>8</sup>. In the framework of an effective action approach, these authors simulate a system undergoing a second order QCD phase transition. The  $\eta$  signal at low  $p_T$  (Fig. 3) is much stronger than seen in HIJING and is dominated by the coarse scale.

## 6. STAR measurements of dynamic textures

Elliptic flow is a prominent large scale dynamic texture effect already well measured at RHIC<sup>9</sup>. The DWT approach localizes elliptic flow on scales 2 and, to some degree, 3 of the azimuthal observables. In this report, we ignore flow and concentrate on the  $\eta$  observables.

Fig. 4 presents the STAR measurements of long range (scale 1) fluctuations in peripheral ( $0.014 < \text{mult}/n_0 < 0.1$ ) collisions and compares

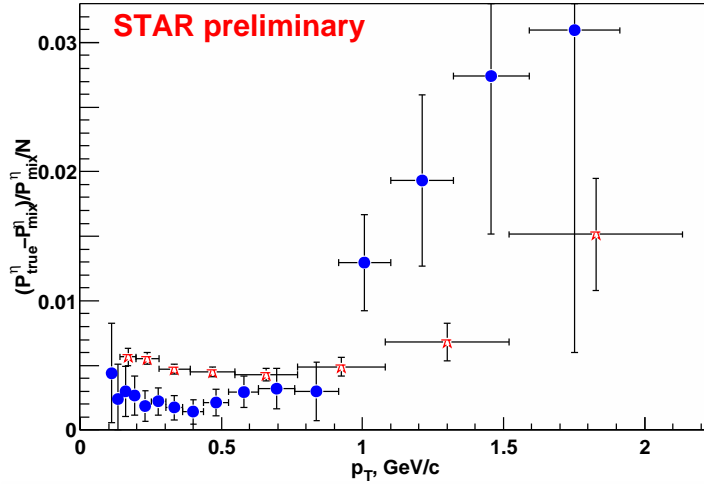


Figure 4.  $(P_{true}^{\eta} - P_{mix}^{\eta})/P_{mix}^{\eta}/N$  for scale 1, peripheral events. Open stars – STAR data for  $\sqrt{s} = 200$  GeV,  $0.014 < \text{mult}/n_0 < 0.1$ . • – HIJING at the same energy,  $\text{mult}/n_0 < 0.1$ .

them with HIJING simulations. Qualitatively, both sets of points behave similarly: a region of nearly flat or falling behavior around mean  $p_T$  is replaced by a rising trend for  $p_T > 0.8$  GeV/c. This trend has already been discussed in Section 5 and is due to jets. The HIJING signal is below the STAR data at low  $p_T$ , but reaches higher values at higher  $p_T$ ; its rise with  $p_T$  is stronger. From this figure we conclude that the fluctuations in local hadron density due to jet production are observable at RHIC in the soft  $p_T$  range ( $p_T < 2$  GeV), and that their *qualitative* features are reasonably well described by a super-position of independent nucleon-nucleon collisions based on the physics learned from  $pp(\bar{p})$  and  $e^+e^-$  experiments at comparable energies. Quantitatively speaking, we keep in mind that due to nuclear shadowing effect<sup>11</sup>, peripheral Au+Au events are not supposed to be identical to elementary collisions. A comparison of  $pp$ , dAu and AuAu data from RHIC will shed more light on this effect. In the absence of experimental data on nuclear shadowing of gluons, HIJING assumes<sup>7</sup> equivalence of the effect for quarks and gluons.

Next look at a central sample (Fig. 5) – there is a remarkable difference: we now see a change in the  $p_T$  trend above  $p_T = 0.6$  GeV. Instead of rising with  $p_T$  (as in the peripheral events), the STAR data points become



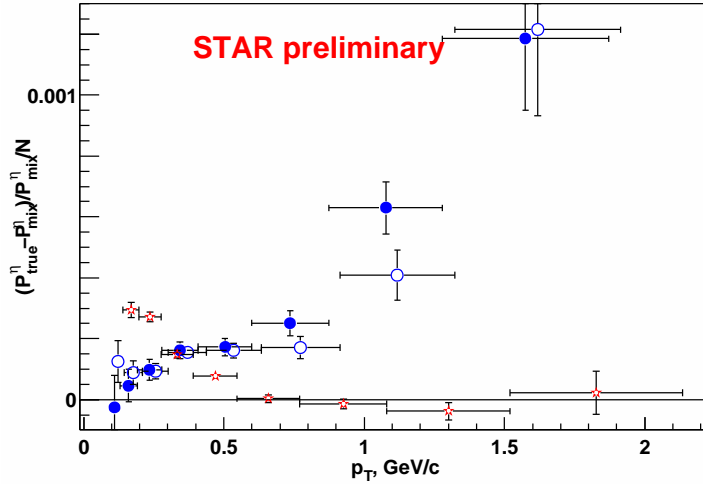


Figure 5.  $(P_{true}^n - P_{mix}^n)/P_{mix}^n/N$  for scale 1, central events ( $0.65 < mult/n_0 < 1.$ ). Open stars – STAR data for  $\sqrt{s} = 200$  GeV. • – regular HIJING; ○ – HIJING with jet quenching, both at  $\sqrt{s} = 130$  GeV.

consistent with 0. The  $p_T$  trends in the data and HIJING look opposite: the model still predicts a monotonic rise with  $p_T$ . Can there be a single explanation to both disappearance of texture at moderate  $p_T$  and its enhancement at low  $p_T$ ? The hypothetical deconfined medium is expected to suppress jet production via dissipative processes (jet quenching)<sup>10</sup>. The medium-induced energy loss per unit of length is proportional to the size of the medium and thus, the effect grows non-linearly with system size. Suppression of hadron yields at high  $p_T$  in central AuAu events with respect to scaled  $pp$  and peripheral collisions has been reported<sup>12</sup> and interpreted as an evidence of medium effects (possibly, nuclear shadowing<sup>11</sup>). Jet quenching is modeled in HIJING, and is seen (compare two sets of HIJING points in Fig.5) to affect the texture observable somewhat. If the dissipation takes place, one may expect that as jets and mini-jets thermalize, the textures associated with them migrate towards mean  $p_T$ . A transport model would be needed in order to simulate such a process. However, the low  $p_T$  fluctuations may have an independent origin, unrelated directly to the partonic energy loss in medium.

## 7. Conclusions

A non-trivial picture of texture effects emerges when the DWT power spectrum technique is applied to AuAu data from RHIC. Long range ( $\Delta\eta \approx 1$ ) pseudo-rapidity fluctuations at soft  $p_T$  are observed in peripheral events and identified with jets and mini-jets. In central events, these fluctuations are not seen, which indicates a change in the properties of the medium. Large scale of the effect points to its early origin. An excess of fluctuations at low  $p_T$  compared to HIJING is seen in peripheral and central events.

## 8. Acknowledgment

I am grateful to Nikos Antoniou and Fotis Diakonou for providing me with simulated phase transition events to establish the sensitivity of the technique to critical phenomena.

## References

1. H. Meyer-Ortmanns, Rev. Mod. Phys. **68**, 473 (1996)
2. I. Bearden *et al.* [NA44], Phys. Rev. C. **65** (2002) 044903
3. I. Daubechies, *Ten Lectures on Wavelets* (SIAM, Philadelphia, 1992) and references therein.
4. K. H. Ackermann *et al.* [STAR], Nucl. Phys. A **661**, 681 (1999) [Nucl. Phys. A **698**, 408 (2002)].
5. C. Adler, A. Denisov, E. Garcia, M. Murray, H. Strobele and S. White, Nucl. Instrum. Meth. A **470**, 488 (2001)
6. G. Uytterhoeven *et al.*, WAILI: Wavelets with Integer Lifting. TW Report 262, Department of Computer Science, Katholieke Universiteit Leuven, Belgium, July 1997.
7. X. N. Wang and M. Gyulassy, Phys. Rev. D **44**, 3501 (1991). M. Gyulassy and X. N. Wang, Comput. Phys. Commun. **83**, 307 (1994)
8. N.G. Antoniou, Y.F. Contoyiannis, F.K. Diakonou, A.I. Karanikas, and C.N. Ktorides, Nucl.Phys.A 693 (2001) 799
9. K. H. Ackermann *et al.* [STAR], Phys. Rev. Lett. **86**, 402 (2001); C. Adler *et al.* [STAR], Phys. Rev. C **66**, 034904 (2002)
10. R. Baier, D. Schiff and B. G. Zakharov, Ann. Rev. Nucl. Part. Sci. **50**, 37 (2000)
11. J. Ashman *et al.* [EMC], Phys. Lett. B **202**, 603 (1988); M. Arneodo *et al.* [EMC], Phys. Lett. B **211**, 493 (1988).
12. K. Adcox *et al.* [PHENIX], Phys. Rev. Lett. **88**, 022301 (2002) C. Adler *et al.* [STAR], Phys. Rev. Lett. **89**, 202301 (2002)